Heterogeneous Catalysis

DOI: 10.1002/anie.201201068

# Tuning the Metal–Adsorbate Chemical Bond through the Ligand Effect on Platinum Subsurface Alloys**

*Toyli Anniyev, Sarp Kaya,* Srivats Rajasekaran, Hirohito Ogasawara, Dennis Nordlund, and Anders Nilsson*

The reactivity of solid surfaces is governed by the local electronic structure.[1] In particular, the role of the valence d electrons to the bond strength of adsorbates on transition metals is emphasized in the d band model developed by Nørskov et al.[2–4] The d band model describes how the chemisorption energy of adsorbates and the average energy of the d electrons with respect to the Fermi level correlate. This arises from the interaction of adsorbate valence electrons with the valence electrons of the transition metals, which leads to formation of bonding and antibonding states; the degree of filling of the latter determines the strength of the adsorption bond. It was further demonstrated that tuning of the d band structure leads to a predictable modification of reactivity in bimetallic systems.[4] There are two major tuning parameters for the electronic structure of a metal surface in a bimetallic system: strain and ligand effects. The strain effect arises from the difference in the nearest neighbor atomic distances at surfaces from those in the pure metals and may include compressed or expanded arrangements of surface atoms.[5] Ligand effects[6] are due to the vicinity of foreign metals around a metal atom that modifies its electronic structure.[7] The strain and ligand effects are generally simultaneously present and produce a combined effect on the catalytic activity in bimetallic catalysis. In a few cases the strain effect can be isolated.[8,9] Subsurface alloys,[10–12] in which a foreign metal layer is confined in the second layer of a host metal, provide an ideal model system for isolating the ligand effect on improved catalytic activity. In these systems, the surface lattice constant is not changed and any changes in the electronic properties of the surface will be due to interaction with the subsurface metal atoms.

The Pt-$M_{3d}$-Pt(111) bimetallic sandwich alloys ($M_{3d}$ = Ni, Co: 3d transition metals) are the best possible candidates to systematically evaluate the ligand effect on adsorbate–surface chemical bonds. These bimetallic alloys have Pt atoms in the topmost layer with unperturbed lattice parameter and a controlled ligand environment in the subsurface region, which varies the energy position of the d band center of the topmost layer.[13] Using atom-specific X-ray spectroscopy of adsorbed oxygen, we provide the direct evidence for ligand-effect-induced changes in the Pt–O chemical bonding in the occupied and unoccupied regions of the electronic structure. We relate the weakening of the Pt–O chemical bond to increased filling of the antibonding states of the chemisorbed oxygen–platinum complex.

The valence-band (VB) X-ray photoelectron spectroscopy (XPS) shown in Figure 1 A confirms the systematic changes in the density of states (DOS) caused by the substitution of subsurface Pt for Ni and Co. The intensity of the states close to the Fermi level (0 eV) decreases and the average energy of the VB shifts towards higher binding energy (BE). In particular, we observe a sharp systematic decrease of the intensity of the peak below the Fermi level and an increase of the intensity at 2.5 and 5 eV. The decrease of the DOS at the Fermi level was accompanied by an increase in the DOS at the lower-energy region of the d band. The resulting redistribution of the DOS, the increased d band width; leads to the downshift of the d band center. The effect was attributed to hybridization between the surface Pt 5d and the subsurface metal 3d bands. The d–d overlap between the Pt 5d and subsurface 3d band was estimated to be larger than that of surface Pt 5d and subsurface Pt 5d on a clean Pt(111), and is due to a decreased layer separation in Pt-$M_{3d}$-Pt(111) system. The d band center shift, calculated as the change in first moment of the VB spectra from that of Pt(111), is $\Delta\varepsilon_d \approx -0.1$ eV for both Pt-$M_{3d}$-Pt(111) surfaces (the small sensitivity towards the kind of metal in the second layer is probably due to the contribution from the d band of the 3d metal, which we estimate to be around 30 % (Supporting Information, Section S3). The peak appearing at 2.5 eV is thus attributed to 3d metal valence states, centroid of which is

[*] T. Anniyev, S. Rajasekaran, A. Nilsson
Stanford Institute for Materials and Energy Sciences
SLAC National Accelerator Laboratory
2575 Sand Hill Rd, Menlo Park, CA 94025 (USA)

T. Anniyev, S. Kaya, S. Rajasekaran, H. Ogasawara, D. Nordlund, A. Nilsson
Stanford Synchrotron Radiation Lightsource
SLAC National Accelerator Laboratory
2575 Sand Hill Rd, Menlo Park, CA 94025 (USA)
E-mail: sarpkaya@slac.stanford.edu

T. Anniyev
Department of Physics, Stanford University
Stanford, CA 94305 (USA)

S. Kaya, A. Nilsson
SUNCAT Center for Interface Science and Catalysis
SLAC National Accelerator Laboratory
2575 Sand Hill Rd, Menlo Park, CA 94025 (USA)

S. Rajasekaran
Department of Material Science and Engineering
Stanford University, Stanford, CA 94305 (USA)

[**] This work is supported by the Department of Energy, Office of Basic Energy Sciences, Division of Materials Sciences and Engineering, under contract DE-AC02-76SF00515. This research was carried out at the Stanford Synchrotron Radiation Lightsource, a national user facility operated by Stanford University on behalf of the U.S. Department of Energy, Office of Basic Energy Sciences.

Supporting information for this article is available on the WWW under http://dx.doi.org/10.1002/anie.201201068.


© 2012 Wiley-VCH Verlag GmbH & Co. KGaA, Weinheim

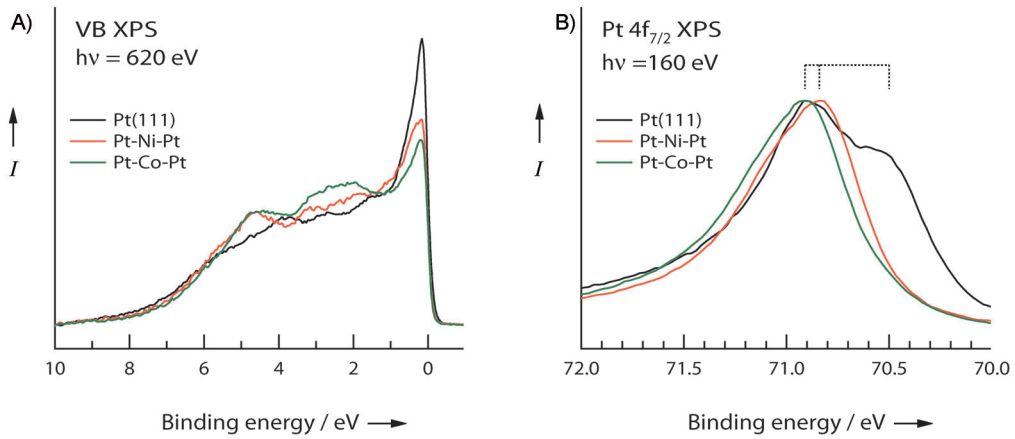


***Figure 1.*** A) Background-subtracted VB XPS spectra comparison between Pt(111) and Pt-$M_{3d}$-Pt(111) ($M_{3d}$ = Ni, Co) structures. The spectra are normalized to the area between 0 and 10 eV. The measurements were carried out at 15° grazing electron emission geometry to enhance the surface sensitivity. B) Pt $4f_{7/2}$ CL XPS spectra; comparison between Pt(111) and Pt-$M_{3d}$-Pt(111) structures. Pt(111) has surface and bulk components with BEs of 70.5 eV and 70.9 eV, respectively. The vertical bars correspond to the position of the peak maxima for Pt-$M_{3d}$-Pt(111) structures and the surface peak of Pt(111).

expected to be further down from the Fermi level owing to alloying.

Density functional theory (DFT) studies predict that[13] the magnitude of the d band center shift increases systematically as the 3d metal is chosen further to the left in the periodic table. These theoretical and our experimental VB results are similar to those obtained in earlier studies on VB electronic structure of alloys which showed a general trend depending on the electronegativity of the metals alloyed with Ni and Pd metals.[14,15] The main emphasis was put on the shifts of the valence states due to d band filling induced by alloy formation and their main contribution to overall valence band structure. Similar to subsurface alloys, the valence band centroid shifts to higher binding energies were larger for electropositive metals (further to the left in the periodic table). One advantage of studying well-ordered subsurface systems over that on random alloys is the ability to isolate the effect due to d band hybridization with partner atoms (ligand effect) from those that are due to a change in number of neighbor atoms and neighbor–neighbor distances.

The d band center shifts are further established by use of surface sensitive Pt 4f core level (CL) XPS shown in Figure 1 B. CL XPS is a complementary tool to VB XPS and has been successfully used to correlate core level shifts to d band center shifts.[16,17] The results clearly indicate the shift of the Pt $4f_{7/2}$ surface peak (70.5 eV) to higher BE consistent with the downshift of the Pt 5d band. The observed Pt 4f BE shifts of 0.34, 0.41 eV (Supporting Information, Section S3) for Pt-Ni-Pt and Pt-Co-Pt samples compare well with the DFT calculated d band center shifts of 0.14 and 0.30 eV.[13] We note that core level binding energy shifts cannot directly be attributed change in d band center owing to possible involvement of final-state core hole screening effects.[18,19] However the order does not change, although absolute energy values might be slightly different.

The strength of the Pt–O bond is identified as an "activity descriptor", which governs the catalytic property of the oxygen reduction reaction activity of Pt-based catalysts.[20] It is quite interesting to capture how the electronic state of Pt–O bond changes upon the d band center shifts. There has been a challenge to separate the electronic states of Pt–O from the dominant substrate Pt states. X-ray emission spectroscopy (XES) and X-ray absorption spectroscopy (XAS) provide the means to probe DOS projected on an atomic site in occupied and unoccupied electronic space. Using oxygen CL resonant XES and XAS, we obtained an oxygen atom projected view of the Pt–O chemical bond.[21,22] Figure 2 shows XES and XAS of oxygen atoms adsorbed on Pt(111) and Pt-$M_{3d}$-Pt(111) bimetallic samples. The spectral intensity of XES and XAS corresponds to Pt–O chemical bond in energy space for occupied and unoccupied states, respectively. XES and XAS measurements performed in two different sample versus photon *E*-vector geometries, in-plane and out-of-plane, correspond to the DOS of O 2p orbital with nodal plane parallel ($p_x, p_y$) and perpendicular ($p_z$) to the sample surface. We indicate the BE scale referenced to the Fermi level, which is obtained by the subtraction of O 1s CL BE with respect to the Fermi level from the X-ray transition energy.[18] The spectral signatures arise from hybridized Pt–O chemical bond derived from Pt 5d and O 2p orbitals, resulting in a bonding and antibonding orbitals of chemisorbed oxygen atoms. The peak at 6 eV in O/Pt(111) XES is assigned to the filled Pt–O bonding states. The antibonding states, which are observed as a shoulder at 2 eV in the XES spectrum, spill over above the Fermi edge and are partially empty and seen in XAS as a resonance at −1 eV. The Pt–O bonding orbitals are at a higher binding energy than the Pt–O antibonding orbitals, and they are the first to fill up. There is an influence of the orbital overlap between Pt and O, which is seen as an anisotropy between the ($p_x, p_y$) and $p_z$ orbitals in Pt–O bonding interaction.[21]

In a fcc hollow site, the largest orbital overlap occurs for p orbitals oriented parallel to the surface, where the O p and Pt surface d orbitals are mostly involved in the σ bond, whereas perpendicular to the surface the bonding is more in π configuration.[23] Since σ interactions induce a stronger overlap between the O 2p and Pt 5d orbitals, the O ($p_x, p_y$) orbitals are affected more by the changes in the surface electronic structure. A smaller orbital overlap between Pt 5d and O $p_z$ orbitals compared to that of O ($p_x, p_y$) orbitals translates to a smaller energy separation between bonding and antibonding states, as observed in the XES and XAS spectra. Whereas the bonding state stays fully occupied, the

 © 2012 Wiley-VCH Verlag GmbH & Co. KGaA, Weinheim 

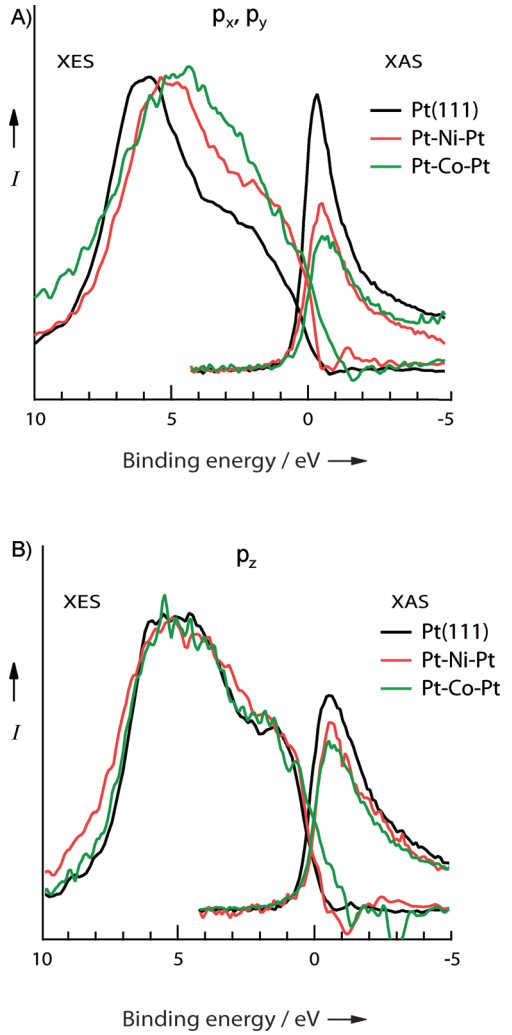


***Figure 2.*** Comparison of oxygen K-edge XES and XAS spectra from oxygen adsorbed on Pt-$M_{3d}$-Pt(111) and Pt(111) surfaces. XES and XAS spectra are shown on a combined binding energy scale to show occupied and unoccupied DOS, respectively. A) In-plane oxygen ($p_x$, $p_y$) and B) out-of-plane oxygen $p_z$ contributions are shown. The XES spectra were normalized to the bonding peak at 6 eV and the XAS spectra were normalized to the edge jump. The scaling between XES and XAS spectra is arbitrary.

occupation of the partially empty antibonding state cutting the Fermi level changes depending on the orbital symmetry. This is well-observed in the energy region between 3 and −2 eV: XAS intensity in $p_z$ bonding symmetry is less pronounced, suggesting that antibonding states are more filled.

By substituting the atoms in the subsurface region from Pt to Ni and Co, we clearly see how the ligand effect modifies the Pt−O chemical bond as observed in XES and XAS. It enhances proportionally the orbital overlap: the changes are more prominent in ($p_x$, $p_y$) symmetry compared to the $p_z$ symmetry. In the ($p_x$, $p_y$) symmetry, we observe three immediate effects for both Pt-$M_{3d}$-Pt(111) surfaces. In XAS, the intensity of the antibonding resonance is drastically reduced. In XES, the position of the bonding peak shifts to lower BE and the intensity of the antibonding shoulder (region between the Fermi level and 5 eV) increases compared to the bonding peak. Although a similar trend is observed, the effect on $p_z$ Pt−O bonding is less pronounced. The ligand effect hardly modifies spectra: the intensity of the antibonding shoulder stays the same in XES spectra and there is a slight decrease in the intensity of XAS resonance. This is reflected in that the σ bond (in-plane) is much stronger and will vary more between the different surfaces than the π bond (out of plane).

In the ($p_x$, $p_y$) projected system, we observe an increase of the relative intensity of the antibonding peak in the XES going from clean Pt(111) to Pt-Co-Pt(111). Within the chemical bonding picture of atomic adsorbates to transition metals,[2–4] the population of the antibonding states has been established as a measure of the adsorbate–metal interaction. If the antibonding state is populated, the net bonding effect cancels out and the interaction becomes repulsive. The results of ($p_x$, $p_y$) projected XAS are complementary to the XES results: the intensity of XAS resonance (antibonding in nature) decreases going from clean Pt(111) to Pt-Co-P(111), which implies that antibonding states become more populated. To quantify the trends of modified Pt ligands on the strength of the Pt−O interaction, we have fitted the O ($p_x$, $p_y$) projected XES with bonding and antibonding contributions (for fitting details, see the Supporting Information, Section S5). We focus here only on the XES spectra, as they are the occupied orbitals that contribute to the bonding. As a measure of the Pt−O bond order, we used the difference between the number of bonding valence p electrons and the number of antibonding valence p electrons, where the number of electrons are the peak areas of the bonding and antibonding peaks in XES (Supporting Information, Section S5). We assume that the polarization between Pt and O in the bonding and antibonding orbitals remains the same; this is mostly different between the two orbitals but still valid to observe trends. We estimate the reduction in Pt−O bond order of about 70% and 55% for Ni- and Co-modified Pt surfaces with respect to Pt(111). This means that due to lower energy position of the surface d band, compared to Pt(111), the Pt−O bond becomes weaker, as more electrons occupy the antibonding orbitals.

We further confirmed that the downshift of the d band center and the population of antibonding state are directly associated with the bond strength of adsorbed hydrogen. Using the fact that the Pt−H bond strength is comparable to the activation energy of thermal desorption of hydrogen, the ligand effect on the Pt−H bond strength will be confirmed through thermal desorption.[12] Figure 3 shows the thermal desorption measurements of $D_2$ from Pt-$M_{3d}$-Pt(111). The downshift of the d band center weakens the bond strength of Pt−D bond, which is seen as a systematic decrease in desorption peak temperature. In the inset of Figure 3, we compared the experimental Pt−D bond energy and the DFT-calculated[13] Pt−H bond energy on Pt-$M_{3d}$-Pt(111) bimetallic surfaces. The experimental trend of $D_2$ desorption barriers agrees well with DFT calculations. This clearly shows that the change in the adsorption properties of the platinum–subsurface bimetallic samples is governed by the change in the electronic structure of the surface Pt layer and scales with the d band center metric.


© 2012 Wiley-VCH Verlag GmbH & Co. KGaA, Weinheim

| Sample | $D_2$ $E_d$ (eV) | $H_2$ $\Delta H_{ads}$[13] (eV)* |
|---|---|---|
| Pt(111) | 0.66 | 0.62 |
| Pt-Ni-Pt(111) | 0.13 | 0.26 |
| Pt-Co-Pt(111) | 0.04 | 0.05 |

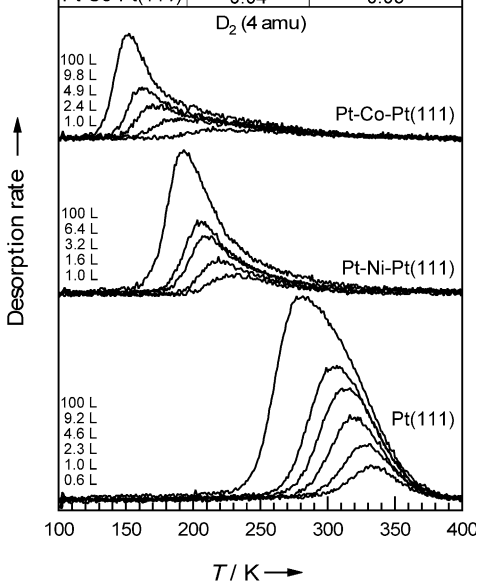


***Figure 3.*** Deuterium ($D_2$) desorption from Pt(111) and Pt-$M_{3d}$-Pt(111) bimetallic surfaces. The $D_2$ exposures are indicated for each sample. The linear heating rate $\beta$ was 3 K $s^{-1}$ for all TPD measurements. Top: A table of desorption barriers for $D_2$ desorption from Pt-$M_{3d}$-Pt(111) surfaces. The desorption barrier was calculated using the Redhead[26] formula corresponding to second order desorption[26] (from the slope of the $\ln(n_0 T_p^2)$ versus $1/T_p$ plot; Supporting Information, Figure S1). (*) The experimental barriers are compared with DFT calculations.

In summary, we have synthesized Pt-$M_{3d}$-Pt(111) ($M_{3d}$ = Co, Ni) bimetallic subsurface alloys, which are designed to show the ligand effect tuned reactivity series in oxygen- and hydrogen-adsorption systems. We depicted how the ligand effect tunes the bond order of Pt–O chemical bond through the oxygen atom projection in the occupied and unoccupied space using XES and XAS. The occupation of Pt–O antibonding state as a tuning parameter of bond order was revealed. We confirmed the reactivity series in the desorption temperature of hydrogen.

## Experimental Section

Experiments were carried out in two separate ultrahigh-vacuum (UHV) chambers at a base pressure below $10^{-10}$ Torr. X-ray spectroscopy measurements were performed at beamline 13–2 at Stanford Synchrotron Radiation Lightsource (SSRL). The elliptically polarized undulator at the beamline allows control of the polarization *E*-vector around the axis of the photon propagation direction. The UHV endstation was equipped with an X-ray emission spectrometer, an electron energy analyzer (Scienta R3000), a two-grid LEED system (SPECS), an ion gun (Omicron), and a quadrupole mass spectrometer (QMS, Hiden HAL-201-RC). The sample was mounted on a liquid nitrogen ($LN_2$) cooled rod and could be rotated around the axis of incoming light with a grazing incidence angle equal to 5°.

The Pt(111) crystal was cleaned by cycles of $Ne^+$ ion bombardment, annealing to 1150 K, and dosing $O_2$ while cooling down (from 800 K to 400 K). The cleaning cycles were repeated until a carbon-free surface was obtained, as confirmed by absence of C and O signals in XPS (indicating contamination levels less than 1% of a monolayer). Heating was achieved using electron bombardment from a 0.15 mm thoriated tungsten filament situated behind the sample. The temperature was measured by chromel–alumel thermocouples spot-welded to the side of the crystal. The surface ordering was confirmed by LEED.

Co and Ni were vapor-deposited on Pt(111) by an e-beam evaporator (Omicron EFM-3) using 2 mm diameter metal rods. All of the rods were purchased from Goodfellow and were 99.99% pure. The low base pressure was maintained during the evaporation. The coverage of the deposited 3d metal was one monolayer (ML) for each admetal. To calibrate the Co deposition rate, the films of gradually increasing coverages were oxidized at 800 K. This produced epitaxial CoO monolayers with distinctive Moiré LEED patterns.[24] Coverage of these oxide layers was calibrated by adsorbing CO on clean Pt(111) terraces at 90 K. The area of clean Pt(111) linearly decreases with oxide coverage, indicating two-dimensional layered growth. Monolayer coverage was judged by complete covering of the Pt(111) by the oxide. Ni deposition rate was estimated by having the same intensity of the 3p core level XPS peak as in the case of Co deposited at room temperature (RT). This was possible because ionization cross-section of 3p states of these metals are close to each other.[25] We prepared Pt-Ni-Pt(111) and Pt-Co-Pt(111) bimetallic sandwich samples by the deposition of 3d metal on Pt(111) at an elevated temperature of 600 K, which leads to the enrichment of Pt in the first layer as a result of the diffusion of 3d metal into the subsurface region.[10,12] We confirmed the bimetallic sandwich structure by depth profiling using XPS.

The atomic oxygen layers on Pt(111) were prepared at RT. We were not successful in chemisorbing oxygen on Pt-Ni-Pt(111) and Pt-Co-Pt(111) at 300 K. Atomic oxygen on these structures was prepared by adsorption of molecular oxygen at 90 K, dissociation by high-flux X-ray irradiation and subsequent annealing to RT. The gas dose was carried out using a pulse gas doser.

Received: February 8, 2012
Published online: June 18, 2012

**Keywords:** bimetallic surface alloys · core level spectroscopy · d band model · heterogeneous catalysis · platinum

[1] S. Roginsky, E. Schulz, *Z. Phys. Chem. Abt. A* **1928**, *138*, 21.
[2] B. Hammer, J. K. Nørskov, *Surf. Sci.* **1995**, *343*, 211.
[3] B. Hammer, J. K. Nørskov in *Advances in Catalysis*, *Vol. 45*, Academic Press Inc, San Diego, **2000**, p. 71.
[4] T. Bligaard, J. K. Nørskov in *Chemical bonding at surfaces and interfaces*, 1st ed. (Eds.: A. Nilsson, L. G. M. Pettersson, J. K. Nørskov), Elsevier, Amsterdam, **2008**, p. 255.
[5] M. Mavrikakis, B. Hammer, J. K. Nørskov, *Phys. Rev. Lett.* **1998**, *81*, 2819.
[6] Y. Gauthier, M. Schmid, S. Padovani, E. Lundgren, V. Buš, G. Kresse, J. Redinger, P. Varga, *Phys. Rev. Lett.* **2001**, *87*, 036103.
[7] P. Liu, J. K. Nørskov, *Phys. Chem. Chem. Phys.* **2001**, *3*, 3814.
[8] A. Schlapka, M. Lischka, A. Groß, U. Käsberger, P. Jakob, *Phys. Rev. Lett.* **2003**, *91*, 016101.
[9] P. Strasser, S. Koh, T. Anniyev, J. Greeley, K. More, C. F. Yu, Z. C. Liu, S. Kaya, D. Nordlund, H. Ogasawara, M. F. Toney, A. Nilsson, *Nat. Chem.* **2010**, *2*, 454.
[10] J. R. Kitchin, N. A. Khan, M. A. Barteau, J. G. Chen, B. Yakshinksiy, T. E. Madey, *Surf. Sci.* **2003**, *544*, 295.
[11] S. Surnev, M. Sock, M. G. Ramsey, F. P. Netzer, B. Klotzer, W. Unterberger, K. Hayek, *Surf. Sci.* **2002**, *511*, 392.
[12] M. P. Humbert, J. G. G. Chen, *J. Catal.* **2008**, *257*, 297.
[13] J. R. Kitchin, J. K. Nørskov, M. A. Barteau, J. G. Chen, *J. Chem. Phys.* **2004**, *120*, 10240.
[14] J. C. Fuggle, F. U. Hillebrecht, R. Zeller, Z. Zolnierek, P. A. Bennett, C. Freiburg, *Phys. Rev. B* **1983**, *27*, 2145.

 © 2012 Wiley-VCH Verlag GmbH & Co. KGaA, Weinheim 

[15] F. U. Hillebrecht, J. C. Fuggle, P. A. Bennett, Z. Zolnierek, C. Freiburg, *Phys. Rev. B* **1983**, *27*, 2179.
[16] M. Weinert, R. E. Watson, *Phys. Rev. B* **1995**, *51*, 17168.
[17] B. Hammer, Y. Morikawa, J. K. Nørskov, *Phys. Rev. Lett.* **1996**, *76*, 2141.
[18] N. Mårtensson, A. Nilsson, *J. Electron Spectrosc. Relat. Phenom.* **1995**, *75*, 209.
[19] I. A. Abrikosov, W. Olovsson, B. Johansson, *Phys. Rev. Lett.* **2001**, *87*, 176403.
[20] J. K. Nørskov, J. Rossmeisl, A. Logadottir, L. Lindqvist, J. R. Kitchin, T. Bligaard, H. Jónsson, *J. Phys. Chem. B* **2004**, *108*, 17886.
[21] A. Nilsson, L. G. M. Pettersson, *Surf. Sci. Rep.* **2004**, *55*, 49.
[22] A. Nilsson, L. G. M. Pettersson, B. Hammer, T. Bligaard, C. H. Christensen, J. K. Nørskov, *Catal. Lett.* **2005**, *100*, 111.
[23] T. Wiell, J. E. Klepeis, P. Bennich, O. Bjorneholm, N. Wassdahl, A. Nilsson, *Phys. Rev. B* **1998**, *58*, 1655.
[24] M. De Santis, A. Buchsbaum, P. Varga, M. Schmid, *Phys. Rev. B* **2011**, *84*, 125430.
[25] J. J. Yeh, I. Lindau, *At. Data Nucl. Data Tables* **1985**, *32*, 1.
[26] P. A. Redhead, *Vacuum* **1962**, *12*, 203.

 © 2012 Wiley-VCH Verlag GmbH & Co. KGaA, Weinheim 